Plasmons and the electromagnetic response of nanowires

Alejandro Jara,[1] R. E. Arias,[1] and D. L. Mills[2]
[1]*Departamento de Física, FCFM, Universidad de Chile, Casilla 487-3, Santiago, Chile*
[2]*Department of Physics and Astronomy, University of California, Irvine, California 92697, USA*
(Received 12 October 2009; revised manuscript received 3 December 2009; published 18 February 2010)

We present a theory of the nature of plasmons in nanowires along with the response of such systems to a spatially uniform applied electric field in the plane perpendicular to the symmetry axis of the wire. We confine our analysis to the electrostatic description of these properties and to modes with infinite wavelength parallel to the wire's symmetry axis. Our theory thus focuses on the limit where the linear dimensions of the cross section are small compared to the wavelength of radiation that may illuminate the system. We derive integral equations that involve only the electrostatic potential on the boundary of the wire for a wire of arbitrary cross section. Once this is solved, a complete description of the potential may be generated. Companion equations are obtained for the function that provides one with the lines of electric field in the system. The homogeneous versions of these equations provide one with a means of finding the plasmon eigenfrequencies and eigenfunctions, whereas the inhomogeneous equations allow one to generate the response of the nanowire to a spatially uniform applied field. We present numerical studies of the plasmon normal modes and electromagnetic response of nanowires of rectangular cross section, and we compare our results to experiments and to a calculation done by other methods.

DOI: 10.1103/PhysRevB.81.085422 PACS number(s): 78.67.−n

I. INTRODUCTION

Currently, there is great interest in the electromagnetic response of diverse nanostructures. Metallic systems are of particular interest because they possess collective modes of the conduction electrons referred to as plasmon modes. When an external source such as a laser excites such a mode, the electric field of the laser may be enhanced greatly in the near vicinity of the nano-object. Thus, for example, one realizes surface enhanced Raman signals wherein the excitation cross section for diverse molecules can be larger than realized in the liquid or gas phase by many orders of magnitude.[1] It is also the case that very large enhancements are realized for diverse nonlinear optical interactions through exploitation of plasmon resonances. The detection of single molecules by optical means is feasible in the presence of such enhancement effects.[2]

Theoretical descriptions of the plasmon modes and electromagnetic response characteristics of diverse nanosystems are thus of interest. In the limit where the relevant linear dimensions of a structure are small compared to the wavelength of the light with which it is illuminated, simplifications in the theory are possible. The electric field in the incident light may be regarded as spatially uniform in the near vicinity of the object, and it is the case as well that the local electric fields set up by electron motions may be described within the framework of electrostatic theory. For very simple structures (a single sphere; a single nanowire of cylindrical cross section), the description of both the electromagnetic response and the plasmon normal modes are elementary within this framework. Through use of special coordinate systems, one can extend the description to somewhat more complex structures. Examples are a sphere placed near a plane[3,4] and two spheres, possibly dissimilar, in near proximity to each other.[5,6] Through use of multiple scattering theory, arrays of spheres[7] or parallel nanowires of circular cross section may be examined.[8]

If one wishes to address objects of more complex shape, even within the simple picture outlined in the previous paragraph, the theory remains a challenge. Consider, for example, a sample in the shape of a rectangular prism or the limiting case of an infinitely long nanowire of rectangular cross section. We note that one finds interesting experimental studies of rectangular nanowires in the literature.[9–11] For such samples, one may expand various quantities of interest inside the material in terms of appropriate Fourier series. However, there are no convenient sets of basis functions for use in the region outside the sample. Thus, the classical method of employing expansions in orthogonal basis functions fails for such a case.

In this class of problems, it is possible to derive eigenvalue equations in the form of integral equations that involve only the relevant potential on the boundary of the medium. Once the potential on the boundary for a particular normal mode is determined, then the extinction theorem of mathematical physics allows one to find the potential associated with a given mode everywhere if desired. Thus, one can describe the nature of the fields set up by charge motions both inside and outside the sample. In the context of the electrostatic theory of plasmons, an elegant approach that leads to such an integral equation has been described by Fredkin and Mayergoyz[12] and by Mayergoyz *et al.*[13] (We would like to direct the reader's attention to most interesting theorems and general statements in Ref. 13.) In a different physical context, the magnetostatic theory of spin waves in ferromagnetic nanowires, two of us have employed the extinction theorem to obtain integral equations of similar form.[14,15] We remark that in the dielectric theory of the response of nanostructures to electric fields, the structures developed in Refs. 14 and 15 allow one to treat gyrotropic media. The virtue of these methods is that they do not require the use of basis functions, either inside or outside the structure of interest. Thus, one can address objects of complex shape.

In this paper, within the context of a method such as that described in the previous paragraph, we address the electrostatic theory of the plasmon normal modes of metallic nanowires of arbitrary cross-sectional shape. We also obtain a description of the response of the wire to a spatially uniform applied electric field. It is the case that the analysis set forth by Fredkin *et al.*[12,13] assumes the dielectric constant of the material of interest to be purely real. In this special limit, one finds infinitely long-lived plasmon modes characterized by real frequencies. Our approach is to begin with the discussion of the response of the system to an external field within the framework of an analysis that allows the frequency-dependent dielectric constant to have both a real and imaginary part. Thus, in our treatment, the effects of dissipation within the sample are taken into account fully within the electrostatic limit. Then one can turn to the idealized case of the nature of the plasmon modes in the absence of dissipation through study of the appropriate limit of the homogeneous equation extracted from our discussion of the response. We also introduce a function analogous to the stream function of hydrodynamics. This describes the lines of electric field associated with the response of the system and satisfies integral equations similar in structure to those satisfied by the electrostatic potential. Construction of the stream function allows one to plot the lines of electric field associated with particular plasmon modes of the structure of interest. We should note that Mayergoyz *et al.*[16] have extended the approach of Refs. 12 and 13 to describe the time evolution of individual plasmon modes of nanoparticles excited by external fields under the circumstance that the dielectric constant of the material is complex. In the discussion we present below, we focus on the frequency-dependent response of nanowires exposed to cw radiation, whereas Ref. 16 explores the response of selected individual modes in the time domain. It is our view that most real materials are sufficiently lossy that the absorption lines with the various modes will overlap, so discussion of selected modes may be of limited interest in practice.

In Sec. II, we derive the integral equations that form the basis for our theory and we also discuss the means we have used to solve them. In Sec. III we present numerical studies of the nature of the plasmon modes of nanowires of rectangular cross section along with calculations of their response to an external electric field. Section IV is devoted to concluding remarks.

II. THEORY

We consider an infinitely long nanowire fabricated from a material with a frequency-dependent complex dielectric constant $\varepsilon(\omega)$. The wire has a constant cross section that may be arbitrary in shape for our purposes at present. The xy plane is perpendicular to the axis of the wire, and in this plane the boundary of the wire is described by a closed curve C. We place the system in a spatially uniform electric field that has frequency ω.

The electric field induces charge motions in the material, and as a consequence there is an electric field everywhere in space which depends on x and y, but which is independent of the coordinate perpendicular to the xy plane. The electric field may be written as

$$\vec{E}(\vec{\rho},t) = \vec{E}_\omega(\vec{\rho})\exp(-i\omega t) + \vec{E}_\omega(\vec{\rho})^*\exp(i\omega t). \tag{1a}$$

The displacement field is $\vec{D}(\vec{\rho},t)=\vec{D}_\omega(\vec{\rho},\omega)e^{-i\omega t}+\text{c.c.}$, and this has the form

$$\vec{D}(\vec{\rho},t) = \varepsilon(\vec{\rho},\omega)\vec{E}_\omega(\vec{\rho},\omega)\exp(-i\omega t) + \varepsilon(\vec{\rho},\omega)^*\vec{E}_\omega(\vec{\rho})^*\exp(i\omega t), \tag{1b}$$

where $\vec{\rho}=x\hat{x}+y\hat{y}$ and we recall that $\varepsilon(\vec{\rho},-\omega)=\varepsilon^*(\vec{\rho},\omega)$. Here $\varepsilon(\vec{\rho},\omega)=\varepsilon(\omega)$ inside the curve C where the nanowire resides and $\varepsilon(\vec{\rho},\omega)=1$ outside C.

Within the electrostatic approximation, we have $\vec{E}(\vec{\rho},t)=-\vec{\nabla}\phi(\vec{\rho},t)$. We view the function ϕ as a function of $z=x+iy$. We introduce a new function $\psi(z,t)$ that everywhere inside and outside z is related to the electrostatic potential by the Cauchy-Riemann conditions

$$\frac{\partial\phi(z,t)}{\partial x} = \frac{\partial\psi(z,t)}{\partial y}, \quad \frac{\partial\phi(z,t)}{\partial y} = -\frac{\partial\psi(z,t)}{\partial x}. \tag{2}$$

We call $\psi(z,t)$ the conjugate potential (or the stream function, to use the terminology of hydrodynamics). One can easily see that inside and outside the nanowire $\vec{E}(\vec{\rho},t)=-\vec{\nabla}\times\psi(\vec{\rho},t)\hat{z}$. We also have the relation $E_x(\vec{\rho},t)-iE_y(\vec{\rho},t)=-\partial\Omega(z,t)/\partial z$, where $\Omega(z,t)=\varphi(z,t)+i\psi(z,t)$ is the complex potential.

We next explore properties of $\Omega(z,t)$. The Cauchy-Riemann conditions ensure that this function is analytic everywhere inside and outside C. The lines of constant ψ are necessarily perpendicular to the equipotential lines everywhere. Thus, the lines of constant ψ are thus the lines of electric field. When we complete our analysis we will obtain two integral equations, one we can solve for $\phi_\omega(z)$ and one we can solve for $\psi_\omega(z)$, where $\phi(z,t)=\phi_\omega(z)\exp(-i\omega t)+\text{c.c.}$ and similarly for $\psi(z,t)$.

Let us suppose we have present an electric field of amplitude $E_0\cos(\omega t)$ that makes the angle θ_0 with the x axis. Such a field is described by the complex potential $\Omega_0(z,t)=-E_0 z\exp(-i\theta_0)\cos(\omega t)$. Our task is then to obtain the total potential as the nanowire responds to this external field.

We shall distinguish between the complex potential inside the nanowire and that outside the nanowire by the notations $\Omega^{in}(z,t)$ and $\Omega^{out}(z,t)$. As noted above, these two functions are analytic in the domain in which they are defined. As one crosses the contour C, the functions display nonanalytic behavior. Clearly $\partial\varphi/\partial n$, the normal derivative of φ, is discontinuous and we will see below that ψ has a jump discontinuity as we cross C. We use the notations z^{in} and z^{out} to denote points inside and outside the nanowire.

Cauchy's theorem gives us the statements

$$\Omega^{in}(z^{in},t) = \frac{1}{2\pi i}\oint_C d\eta\frac{\Omega^{in}(\eta,t)}{\eta - z^{in}} \tag{3a}$$

and also

$$0 = \frac{1}{2\pi i}\oint_C d\eta \frac{\Omega^{in}(\eta,t)}{\eta - z^{out}}. \tag{3b}$$

(The sense of circulation around C and C_∞ is counterclockwise.)

If C_∞ is a circle of very large radius R, where we will let R approach infinity, then we also have

$$\Omega^{out}(z^{out},t) = -\frac{1}{2\pi i}\oint_C d\eta \frac{\Omega^{out}(\eta,t)}{\eta - z^{out}} + \frac{1}{2\pi i}\oint_{C_\infty} d\eta \frac{\Omega^{out}(\eta,t)}{\eta - z^{out}}, \tag{4a}$$

$$0 = -\frac{1}{2\pi i}\oint_C d\eta \frac{\Omega^{out}(\eta,t)}{\eta - z^{in}} + \frac{1}{2\pi i}\oint_{C_\infty} d\eta \frac{\Omega^{out}(\eta,t)}{\eta - z^{in}}. \tag{4b}$$

In Eq. (4), in the integrals over C_∞ one may replace $\Omega^{out}(\eta,t)$ by $\Omega_0(\eta,t)$. The integral is then elementary, so Eq. (4) becomes

$$\Omega^{out}(z^{out},t) = -\frac{1}{2\pi i}\oint_C d\eta \frac{\Omega^{out}(\eta,t)}{\eta - z^{out}} - E_0 z e^{-i\theta_0}\cos\omega t, \tag{5a}$$

$$0 = -\frac{1}{2\pi i}\oint_C d\eta \frac{\Omega^{out}(\eta,t)}{\eta - z^{in}} - E_0 z e^{-i\theta_0 t}\cos\omega t. \tag{5b}$$

Now we make a special choice of both z^{in} and z^{out}. Let z^{in} become $z^<$, a point infinitesimally close to the contour C, but just inside of it. We distort the contour C by including in it a semicircle of very small radius ε centered on $z^<$. After this is done, we may allow $z^<$ to approach a point on the curve C which we denote by ζ. Equation (3a) then becomes (this amounts to the use of Plemelj's formulas)

$$\Omega^{in}(\zeta,t) = \frac{1}{2}\Omega^{in}(\zeta,t) + \frac{1}{2\pi i}\oint_{\text{P.V.}} d\eta \frac{\Omega^{in}(\eta,t)}{\eta - \zeta} \tag{6a}$$

$$\text{or} \quad \Omega^{in}(\zeta,t) = \frac{1}{\pi i}\oint_{\text{P.V.}} d\eta \frac{\Omega^{in}(\eta,t)}{\eta - \zeta}. \tag{6b}$$

Notice that a similar treatment of Eq. (3b) leads also to Eq. (6b). In Eq. (6), the integrals are around the contour C, but now they are principal value integrals. We may treat Eq. (5b) in a similar manner. These do provide the statement

$$\Omega^{out}(\zeta,t) = -\frac{1}{i\pi}\oint_{\text{P.V.}} d\eta \frac{\Omega^{out}(\eta,t)}{\eta - \zeta} - 2E_0 e^{-i\theta_0}\zeta\cos\omega t. \tag{7}$$

We may write $\Omega^{in,out}(\zeta,t) = \Omega^{in,out}_{+\omega}(\zeta)e^{-i\omega t} + \Omega^{in,out}_{-\omega}(\zeta)e^{+i\omega t}$, so we have

$$\Omega^{in}_{\pm\omega}(\zeta) = \frac{1}{i\pi}\oint_{\text{P.V.}} d\eta \frac{\Omega^{in}_{\pm\omega}(\eta)}{\eta - \zeta}, \tag{8a}$$

$$\Omega^{out}_{\pm\omega}(\zeta) = -\frac{1}{i\pi}\oint_{\text{P.V.}} d\eta \frac{\Omega^{out}_{\pm\omega}(\eta)}{\eta - \zeta} - E_0 e^{-i\theta}\zeta. \tag{8b}$$

We next consider the boundary conditions satisfied by the functions that enter Eq. (8). Of course, the electrostatic potential is continuous across the boundary, so $\varphi^{in}_{\pm\omega}(\zeta) = \varphi^{out}_{\pm\omega}(\zeta)$ while the normal derivative is discontinuous. We have $\varepsilon(\pm\omega)\partial\varphi^{in}_{\pm\omega}(\zeta)/\partial n = \partial\varphi^{out}_{\pm\omega}(\zeta)/\partial n$. Now we have the Cauchy-Riemann conditions stated in Eq. (2) that apply everywhere. Hence, on the boundary, $\partial\varphi^{in,out}_{\pm\omega}(\zeta)/\partial n = \partial\psi^{in,out}_{\pm}(\zeta)/\partial\tau$ and $\partial\varphi^{in,out}_{\pm\omega}(\zeta)/\partial\tau = -\partial\psi^{in,out}_{\pm}(\zeta)/\partial n$. Here $\partial/\partial\tau$ is the tangential derivative. From these relations, we deduce that $\varepsilon(\pm\omega)\partial\psi^{in}_{\pm\omega}(\zeta)/\partial\tau = \partial\psi^{out}_{\pm\omega}(\zeta)/\partial\tau$, from which it follows that $\varepsilon(\pm\omega)\psi^{in}_{\pm\omega}(\zeta) = \psi^{out}_{\pm\omega}(\zeta)$. We also have continuity of $\partial\psi_{\pm\omega}/\partial n$ across the boundary.

Through use of the boundary conditions, we may write Eqs. (8a) and (8b) as

$$\varphi^{in}_{+\omega}(\zeta) + i\psi^{in}_{+\omega}(\zeta) = \frac{1}{i\pi}\oint_{\text{P.V.}} d\eta \frac{\varphi^{in}_{+\omega}(\eta) + i\psi^{in}_{+\omega}(\eta)}{\eta - \zeta}, \tag{9a}$$

$$\varphi^{in}_{+\omega}(\zeta) + i\varepsilon(\omega)\psi^{in}_{+\omega}(\zeta) = -\frac{1}{i\pi}\oint_{\text{P.V.}} d\eta \frac{\varphi^{in}_{+\omega}(\eta) + i\varepsilon(\omega)\psi^{in}_{+\omega}(\eta)}{\eta - \zeta} - E_0 e^{-i\theta_0}\zeta. \tag{9b}$$

In a similar manner, from Eq. (8), one may obtain analogous integral equations which link $\varphi^{in}_{-\omega}$ and $\psi^{in}_{-\omega}$. Upon noting that $\varphi^{in}_{-\omega}(\zeta) = [\varphi^{in}_{+\omega}(\zeta)]^*$, $\psi^{in}_{-\omega}(\zeta) = [\psi^{in}_{+\omega}(\zeta)]^*$, and $\varepsilon(-\omega) = [\varepsilon(\omega)]^*$, one may take the complex conjugate of these equations to find

$$\varphi^{in}_{+\omega}(\zeta) - i\psi^{in}_{+\omega}(\zeta) = -\frac{1}{i\pi}\oint_{\text{P.V.}} d\eta^* \frac{\varphi^{in}_{+\omega}(\eta) - i\psi^{in}_{+\omega}(\eta)}{(\eta - \zeta)^*}, \tag{9c}$$

$$\varphi^{in}_{+\omega}(\zeta) - i\varepsilon(\omega)\psi^{in}_{+\omega}(\zeta) = +\frac{1}{i\pi}\oint_{\text{P.V.}} d\eta^* \frac{\varphi^{in}_{+\omega}(\eta) - i\varepsilon(\omega)\psi^{in}_{+\omega}(\eta)}{(\eta - \zeta)^*} - E_0 e^{+i\theta_0}\zeta^*. \tag{9d}$$

Upon multiplying Eq. (9a) by $\varepsilon(\omega)$ and adding it to Eq. (9b), one has

$$[1 + \varepsilon(\omega)]\varphi^{in}_{+\omega}(\zeta) + 2i\varepsilon(\omega)\psi^{in}_{+\omega}(\zeta) = \frac{[\varepsilon(\omega) - 1]}{i\pi}\oint_{\text{P.V.}} d\eta \frac{\varphi^{in}_{+\omega}(\eta)}{\eta - \zeta} - E_0 e^{-i\theta_0}\zeta, \tag{10a}$$

whereas a similar manipulation with Eqs. (9c) and (9d) gives us

$$[1 + \varepsilon(\omega)]\varphi^{in}_{+\omega}(\zeta) - 2i\varepsilon(\omega)\psi^{in}_{+\omega}(\zeta) = -\frac{[\varepsilon(\omega) - 1]}{i\pi}\oint_{\text{P.V.}} d\eta^* \frac{\varphi^{in}_{+\omega}(\eta)}{(\eta - \zeta)^*} - E_0 e^{i\theta_0}\zeta^*. \tag{10b}$$

Upon adding Eq. (10b) to Eq. (10a), we obtain the integral equation we seek:

$$\varphi_{+\omega}^{in}(\zeta) = \left[\frac{\varepsilon(\omega)-1}{\varepsilon(\omega)+1}\right]\frac{1}{2\pi i}\left[\oint_{\text{P.V.}} d\eta \frac{\varphi_{+\omega}^{in}(\eta)}{\eta-\zeta} - \oint_{\text{P.V.}} d\eta^* \frac{\varphi_{+\omega}^{in}(\eta)}{(\eta-\zeta)^*}\right] - \frac{E_0}{[1+\varepsilon(\omega)]}\text{Re}(\zeta e^{-i\theta_0}). \tag{11}$$

Similar manipulations produce an integral equation satisfied by $\psi_{+\omega}^{in}(\zeta)$:

$$\psi_{+\omega}^{in}(\zeta) = -\left[\frac{\varepsilon(\omega)-1}{\varepsilon(\omega)+1}\right]\frac{1}{2\pi i}\left[\oint_{\text{P.V.}} d\eta \frac{\psi_{+\omega}^{in}(\eta)}{\eta-\zeta} - \oint_{\text{P.V.}} d\eta^* \frac{\psi_{+\omega}^{in}(\eta)}{(\eta-\zeta)^*}\right] - \frac{E_0}{[1+\varepsilon(\omega)]}\text{Im}(\zeta e^{-i\theta_0}). \tag{12}$$

This completes our general analysis. Our next task is to discuss the means of solving the integral equations just derived. However, before we do this, we comment on the relationship between our analysis and that presented in Ref. 13, where the formalism developed there was applied to the particular case of nanowires. These authors confined their attention to the calculation of the plasmon frequencies of various nanostructures under the assumption that the dielectric function is real. We may obtain an eigenvalue equation for this purpose from the homogeneous version of Eq. (11). We wish to rewrite this in a form which may be compared with the discussion in Ref. 13. Suppose the contour C is described by the relation $y=f(x)$. Then if $\eta=x'+iy'$ and $\zeta=x+iy$, $d\eta=dx'+idy'=[1+if'(x')]dx'$, where $f'=df/dx$. Then if, as earlier, $\vec{\rho}=x\hat{x}+y\hat{y}$, one has

$$\frac{d\eta}{\eta-\zeta} - \frac{d\eta^*}{(\eta-\zeta)^*} = \frac{2i[(x'-x)f'(x')-(y'-y)]}{|\vec{\rho}-\vec{\rho}'|^2}dx'. \tag{13}$$

The outward normal to the contour C is $\hat{n}=[1+f'(x)^2]^{-1/2}\times\{-\hat{x}f'(x)+\hat{y}\}$ and the element of length along C is $dl=[1+f'(x)^2]^{1/2}dx$, so our eigenvalue equation [Eq. (11) with $E_0=0$] has the form

$$\varphi_{+\omega}^{in}(x,y) = \frac{1}{\pi}\left[\frac{\varepsilon(\omega)-1}{\varepsilon(\omega)+1}\right]\oint_{\text{P.V.}} \frac{\hat{n}'\cdot[\vec{\rho}'-\vec{\rho}]}{|\vec{\rho}'-\vec{\rho}|^2}\varphi_{+\omega}^{in}(x'y')dl'. \tag{14}$$

The statement in Eq. (14) is identical to Eq. (47) of Ref. 13.

We could also derive an eigenvalue equation for the conjugate potential ψ from Eq. (12). It would be identical in structure to Eq. (14) except the ratio $\lambda(\omega)=[\varepsilon(\omega)-1]/[\varepsilon(\omega)+1]$ is replaced by its negative. Thus, if $\lambda(\omega_\alpha)=\lambda_\alpha$ is an eigenvalue of Eq. (14), it follows that $-\lambda_\alpha$ is also an eigenvalue. This theorem is proved in Ref. 13 and also follows from the structure we have developed here.

We turn next to the means we use to solve the integral equations derived above. First, we note that the singularity that appears at $\zeta=\eta$ is most inconvenient from the point of view of numerical computation. We may eliminate this by writing

$$\frac{1}{2\pi i}\int_{\text{P.V.}} d\eta \frac{\varphi_{\omega}^{in}(\eta)}{\eta-\zeta} = \frac{1}{2\pi i}\int d\eta \frac{\varphi_{\omega}^{in}(\eta)-\varphi_{\omega}^{in}(\zeta)}{\eta-\zeta} + \frac{\varphi_{\omega}^{in}(\zeta)}{2\pi i}\int_{\text{P.V.}} \frac{d\eta}{\eta-\zeta}. \tag{15}$$

Upon noting $\frac{1}{2\pi i}\int_{\text{P.V.}}\frac{d\eta}{\eta-\zeta}=\frac{1}{2}$, Eq. (11) may be rewritten as

$$\varphi_{\omega}^{in}(\zeta) = \frac{[\varepsilon(\omega)-1]}{4\pi i}\left[\oint d\eta \frac{\varphi_{\omega}^{in}(\eta)-\varphi_{\omega}^{in}(\zeta)}{\eta-\zeta} - \oint d\eta^* \frac{\varphi_{\omega}^{in}(\eta)-\varphi_{\omega}^{in}(\zeta)}{(\eta-\zeta)^*}\right] - \frac{E_0}{2}\text{Re}(\zeta e^{-i\theta}). \tag{16}$$

Equation (12) may be transformed similarly. It is possible to either find the eigenvalues of the homogeneous version of Eq. (16) or to solve the inhomogeneous version by approximating the integrals by a discrete set of points on the boundary and then converting the problem to that of diagonalizing or inverting the appropriate matrix. We have found excellent convergence may be obtained by an alternate approach, wherein the contour integrals in Eq. (16) are converted from integrals over the actual circumference of the nanowire to a circle in a different complex plane.

This is achieved by introducing a mapping of the region outside the nanowire onto the exterior of a circle in a different complex plane we denote as the χ plane. We have $\chi=\upsilon+i\phi$, where ν and ϕ are the radial and angular coordinates in the χ plane. A circle in this plane is described by the statement $\nu=\nu_0$. As discussed by DiPerna and Stanton,[17] a suitable transformation has the form

$$z(\chi) = g_{-1}e^{\chi} + \sum_{n=0}^{\infty} g_n e^{-n\chi}. \tag{17}$$

The authors of Ref. 16 discuss the means of determining the set of coefficients $\{g_n\}$ which appear in Eq. (17) for any choice of nanowire shape. In what follows, we shall assume these coefficients are known. Then we may convert the integrals in Eq. (16) to integrals over ϕ by writing $d\eta=(d\eta/d\phi)d\phi$, where

$$\frac{d\eta}{d\phi} = \frac{d\eta}{d\chi}\frac{d\chi}{d\phi} = i\left[g_{-1}e^{\upsilon_0+i\phi} - \sum_{n=0}^{\infty} n g_n e^{-n\upsilon_0-in\phi}\right]. \tag{18}$$

On the circle in the χ plane, we may write $\varphi_{\omega}^{in}(\eta)=\Sigma_l\varphi_{\omega}^{in}(l)e^{il\phi}$. If this expansion is inserted into the integrals in Eq. (16), then one obtains a set of matrix equations with the form

$$\varphi_{\omega}^{in}(j) = \frac{\varepsilon(\omega)-1}{8\pi^2 i}\int_0^{2\pi} d\phi \int_0^{2\pi} d\phi' e^{-ij\phi}\left\{\sum_l \varphi_{\omega}^{in}(l)(e^{il\phi'} - e^{il\phi})\right]\left[\frac{d\eta(\phi')/d\phi'}{\eta(\phi')-\eta(\phi)} - \text{c.c.}\right]\right\} - \frac{E_0}{4\pi}\int_0^{2\pi} d\phi e^{-ij\phi}\,\text{Re}[\eta(\phi)e^{-i\theta_0}]. \tag{19}$$

To carry out the procedure just set forth, one must evaluate a set of integrals of the form

$$I(j,i) = \int_0^{2\pi} d\phi \int_0^{2\pi} d\phi' e^{-ij\phi} \left[\frac{e^{il\phi'} - e^{il\phi}}{\eta(\phi') - \eta(\phi)} \right] \frac{d\eta(\phi')}{d\phi'} \tag{20}$$

along with a set of integrals where η is replaced by its complex conjugate. These integrals may be calculated numerically through use of fast Fourier transforms.

III. RESULTS AND DISCUSSION

In this section, we describe a series of calculations of the character of the plasmon normal modes of rectangular nanowires and also of their response to a spatially uniform electric field applied parallel to the long dimension of the cross section. Before we present these results, we briefly review general aspects of the structure of the formalism developed in Sec. II.

First, note that the eigenvalues we determine from the homogeneous form of the integral equation in Eq. (11) are the values $\{\lambda_\alpha\}$ of $\lambda(\omega)=[\varepsilon(\omega)-1]/[\varepsilon(\omega)+1]$ for which the homogeneous equation admits a solution. Furthermore, it is evident that λ_α are real. If we consider a model of a material wherein the dielectric function $\varepsilon(\omega)$ is assumed to be real, then the frequencies ω_α of the modes are real; the plasmon modes have infinite lifetime in such a picture. We can also apply the theory to a material wherein dissipation is present. This means that when ω is real, the dielectric constant $\varepsilon(\omega)=\varepsilon_1(\omega)+i\varepsilon_2(\omega)$ is a complex number. Let us suppose that the real number ε_α is an eigenvalue of Eq. (11), where $\lambda_\alpha=(\varepsilon_\alpha-1)/(\varepsilon_\alpha+1)$. Then the "frequency" ω_α of the plasmon mode associated with this value of the dielectric constant is complex. It is found from the relation $\varepsilon(\omega_\alpha)=\varepsilon_\alpha$. The inverse of the imaginary part of the complex frequency ω_α so determined serves as a measure of the lifetime of the plasmon mode α. To determine such a complex frequency numerically, one must know the dielectric function not just along the real axis of the complex frequency plane, but in its upper half as well. In principle, one may use the Kramers-Kronig relations as a means of analytically continuing the dielectric function off the real axis into the upper half of the frequency plane. Such a procedure, while possible in principle to implement, will not be simple.

We have also seen that if λ_α is an eigenvalue, as pointed out by the authors of Ref. 13, $-\lambda_\alpha$ is as well. Thus, if ε_α is an eigenvalue, so is $1/\varepsilon_\alpha$. A pair of modes related in this manner will be referred to as twin modes, to use the language of Ref. 13. From Eqs. (11) and (12), we can see that $\varphi_\omega(z)|_{\varepsilon_\alpha} = \psi_\omega(z)|_{1/\varepsilon_\alpha}$ and $\psi_\omega(z)|_{\varepsilon_\alpha} = \varphi_\omega(z)|_{1/\varepsilon_\alpha}$. That is, the equipotential lines of one member of a twin become the electric field lines of its partner, and conversely.

We now turn to the results of our numerical studies. We begin with the plasmon modes of a rectangular nanowire with an aspect ratio of 2:1. Each mode of such a structure may be labeled with two quantum numbers (σ,σ'), each of which assumes the value +1 or −1. The first number refers to the parity of the equipotential lines with respect to reflection through the x axis and the second to the parity with respect to reflection through the y axis. We note that in metals, the real part of the dielectric constant is negative in the regime where the plasmon normal modes are found by virtue of the contribution from intraband contributions that provide the contribution $-(\omega_p/\omega)^2$, with ω_P the plasma frequency of the conduction electrons. Thus, the lowest frequency mode of the system will have the most negative dielectric constant in the eigenvalue spectrum, and as we move upward in the sequence of ε_α's which emerge from the eigenvalue analysis, the frequencies will increase monotonically. In what follows, we then arrange the information we present in order of the eigenvalue ε_α, with the most negative first.

TABLE I. The eigenvalue spectrum ε_α for a rectangular nanowire with aspect ratio of 2:1. As discussed in the text, the value $\varepsilon_\alpha=-1$ is an accumulation point of the eigenvalue spectrum, so we give only a finite number of eigenvalues in the table below.

−2.6555	−0.9850
−2.3164	−0.9843
−2.2576	−0.9717
−1.9856	−0.9693
−1.6858	−0.9548
−1.3253	−0.9505
−1.3092	−0.9122
−1.2459	−0.9120
−1.1835	−0.8937
−1.1189	−0.8450
−1.0965	−0.8026
−1.0962	−0.7638
−1.0520	−0.7545
−1.0474	−0.5932
−1.0316	−0.5036
−1.0291	−0.4429
−1.0159	−0.4317
−1.0152	−0.3766

In Table I we present the eigenvalues that emerge from our numerical study of the rectangular nanowire with the aspect ratio of 2:1. The results are arranged in two columns. The left-hand column gives eigenvalues for which $\varepsilon_\alpha<-1$ and the right-hand column gives those for which $\varepsilon_\alpha>-1$. We find that $\varepsilon_\alpha=-1$ is an accumulation point of the eigenvalue spectrum. For physical reasons we shall appreciate shortly, it is the case that $\varepsilon_\alpha=-1$ will be an accumulation point of the eigenvalue spectrum for a nanowire of any cross-sectional shape within continuum theory. We only give a finite number of eigenvalues in Table I. Close to the accumulation point it is difficult to determine the eigenvalues numerically.

We turn next to a discussion of the nature of the various normal modes whose eigenvalues are summarized in Table I. We illustrate the four lowest lying modes in Fig. 1; the modes are ordered in terms of the value of the dielectric function eigenvalue ε_α, with the largest negative eigenvalue first. Figure 1(a) shows both the equipotential lines (dark blue/light blue) and electric field lines (red/yellow) of the lowest frequency mode corresponding to $\varepsilon_\alpha=-2.6555$. It is

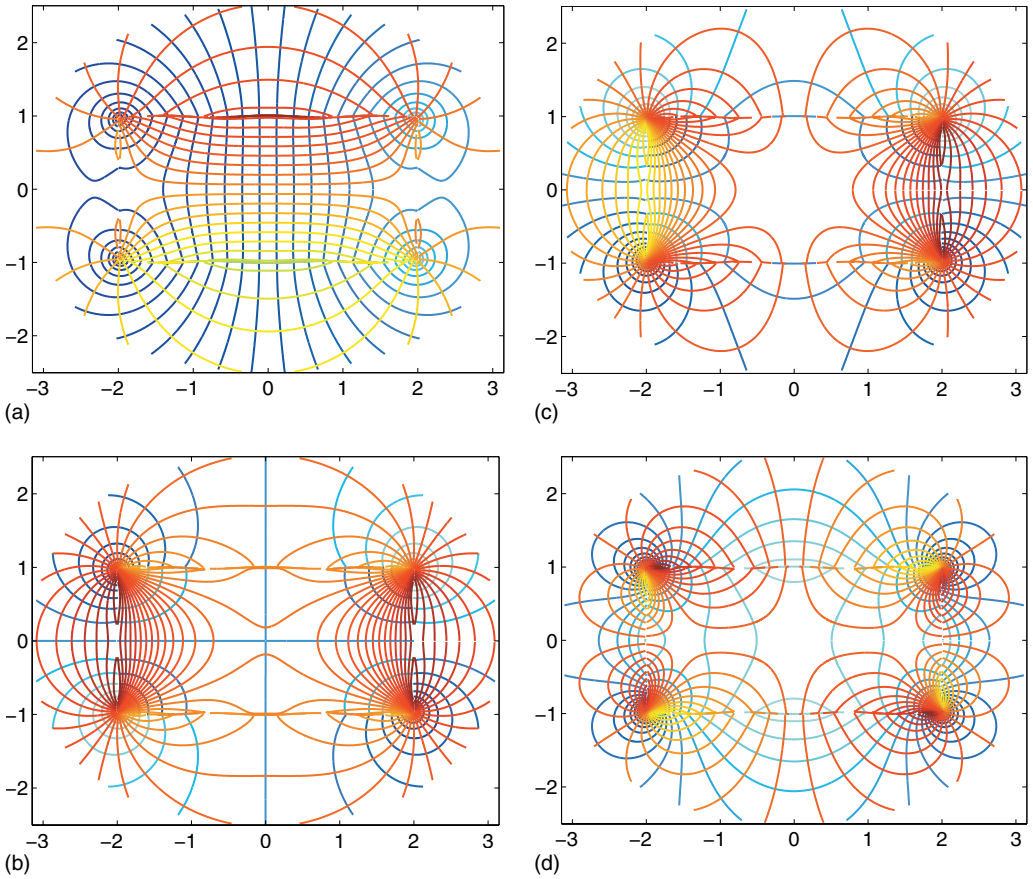

FIG. 1. (Color) The equipotential lines (dark blue/light blue) and lines of electric field (red/yellow) for the four lowest lying plasmon modes of a rectangular nanowire with aspect ratio of 2:1. The eigenvalues represented are (a) $\varepsilon_\alpha=-2.6555$, (b) $\varepsilon_\alpha=-2.3164$, (c) $\varepsilon_\alpha=-2.2576$, and (d) $\varepsilon_\alpha=-1.9856$.

evident that the electric field lines throughout the slab are roughly parallel to the surfaces of the slab. In the metal, one can think of this mode as the mode in which the conduction electrons are sloshing about nearly parallel to the long dimension of the rectangle. In terms of the symmetry classification mentioned above, this mode has the quantum numbers $(+1,-1)$. Clearly this mode will be excited by an electric field applied parallel to the long surfaces of the slab and "silent" if the electric field is perpendicular to the long dimension.

A most striking feature of Fig. 1(a) is that there are polarization charges located at each corner of the slab. These are point charges so far as we can see from our calculation, though we have been unable to obtain precision sufficient to allow us to determine the nature of the singularity in the electrostatic potential as one approaches a corner. For this particular mode the point charges on the two left-hand corners have the opposite sign as those on the right-hand corners. It is trivial to see that the polarization charge density $\rho_{pol}=-\vec{\nabla}\cdot\vec{P}$ integrated over all space must be zero, where $\vec{P}$ is the electric dipole moment per unit volume. Thus, the nanowire must always be electrically neutral, in the sense that ρ_{pol} must always integrate to zero. (Notice that these electrostatic modes have only surface charges.) For all the modes for which $\varepsilon_\alpha<-1$, we find a point polarization charge localized at each corner for each of the normal modes.

In Fig. 1(b), we show the equipotential lines and the lines of electric field for the next highest mode for which $\varepsilon_\alpha=-2.3164$ and in Fig. 1(c) we show the contours for the mode for which $\varepsilon_\alpha=-2.2576$. These modes have quantum numbers $(-1,-1)$ and $(-1,+1)$, respectively. As in Fig. 1(a), the point polarization charges at the corners stand out as very strong features.

In Fig. 1(d), we show the fourth mode for which $\varepsilon_\alpha=-1.9856$. The quantum numbers of this mode are $(+1,+1)$, which means that the polarization charges on each of the four corners are equal in magnitude and sign to each other. As noted above, the system must be electrically neutral. This is addressed by the formation of charges in the center of each side of the rectangle that have sign opposite to that of the four corner charges.

As the eigenvalues ε_α increase toward -1, more and more charges are found arrayed around the boundary of the nanowire. A measure of this is found in the number of zeros or nodes in the electrostatic potential as one makes a circuit around the periphery of the wire. As one moves up in the sequence of normal modes as ε_α progresses to -1, four new zeros are added with each move up the ladder, one on each edge of the periphery.

We illustrate the nature of the higher modes in Fig. 2, where we display the equipotential and field contours for two of the modes. We see clearly that as ε_α progresses toward -1,

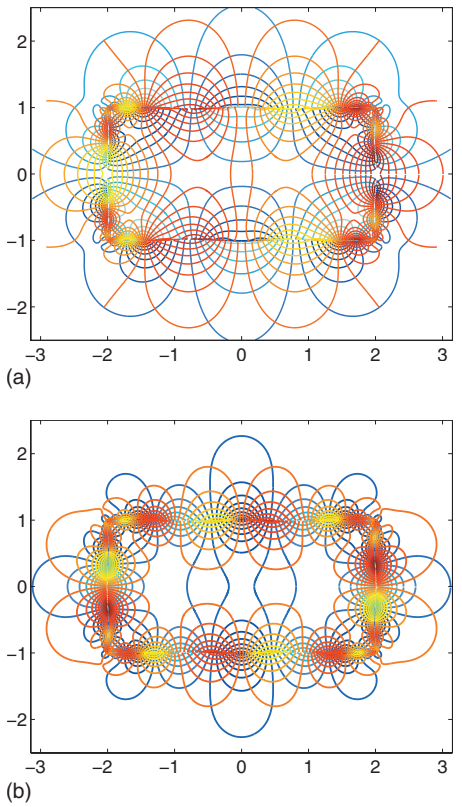

FIG. 2. (Color) For the rectangular nanowire with a cross section of 2:1, we show the equipotential lines (dark blue/light blue) and electric field lines (red/yellow) for two selected plasmon modes. The eigenvalues are (a) $\varepsilon_\alpha=-1.0965$ and (b) $\varepsilon_\alpha=-1.0152$.

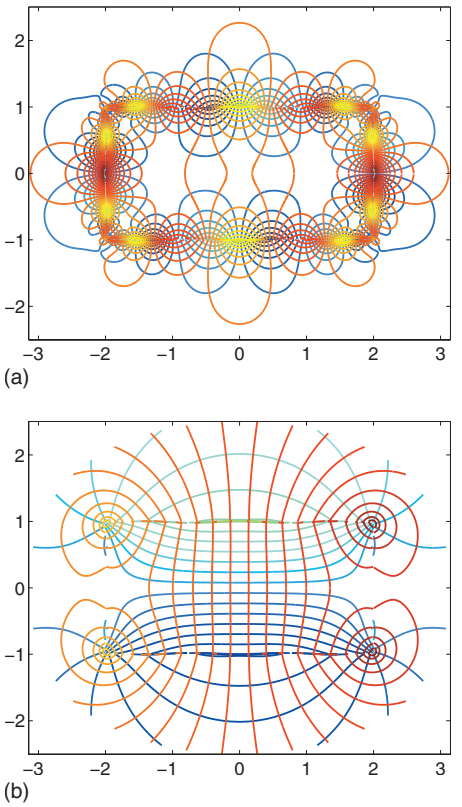

FIG. 3. (Color) The equipotential lines (dark blue/light blue) and the electric field lines (red/yellow) of the plasmon modes corresponding to the eigenvalues (a) $\varepsilon_\alpha=-0.9850$ and (b) $\varepsilon_\alpha=-0.3766$.

more and more charges are arrayed around the circumference.

We have seen above that if ε_α is an eigenvalue, so is $1/\varepsilon_\alpha$. We thus have an infinite sequence of eigenvalues in the region $-1<\varepsilon_\alpha<0$, and again -1 is an accumulation point now approached from above. As we have seen if we examine the set of equipotential lines for the eigenvalue $\varepsilon_\alpha<-1$, these become the electric field lines for the eigenvalue $1/\varepsilon_\alpha>-1$ and conversely. We illustrate this in Fig. 3(a), where we show the equipotential and electric field lines for the mode with $\varepsilon_\alpha=-0.9850$. This mode is the twin of the mode illustrated in Fig. 2(b). Then in Fig. 3(b) we show the mode that corresponds to the eigenvalue $\varepsilon_\alpha=-0.3766$, which is the twin to the mode illustrated in Fig. 1(a).

There are two features of interest in Figs. 3(a) and 3(b). The first can be seen most clearly in Fig. 3(b). We no longer have point charges located at each corner of the periphery of the nanowire. The electric field lines encircle each corner, whereas now the equipotential lines radiate outward. Close examination of the potential near the corners shows that we have two equal and opposite charges that form a point dipole, as opposed to a point charge. We find point dipoles located on the corners for all modes for which $-1<\varepsilon_\alpha<0$. The second point is illustrated best by comparing Fig. 3(a) with the twin of this mode in Fig. 2(b). In Fig. 2(b), the electric field lines are odd under reflection through the x axis, while in Fig. 3(a) they are even under this reflection. The converse is true of the equipotential lines.

We can illustrate some of the points encountered in the discussion above through discussion of a simple example, a plane of dielectric material of thickness D. Let its surfaces be parallel to the xz plane, with the y axis normal to the surfaces, which are infinite in extent. We may regard this system as the limit of a nanowire of rectangular cross section as the aspect ratio approaches infinity. It is, of course, an elementary matter to find the implicit dispersion relation of the plasmons in such a film. Let the surfaces of the film be described by $y=\pm D/2$. Then electrostatic theory admits standing wave solutions for surface plasmons in which all quantities are proportional to $\cos(Qx)\exp(-i\omega_Q^{\pm}t)$. Inside the film one has solutions where the electrostatic potential is odd under reflection through the x axis and thus has a y dependence given by $\sinh(Qy)$. There are even parity solutions in which the potential varies as $\cosh(Qy)$. In both cases, outside the film the potential decays exponentially as $\exp(-Q|y|)$ as one moves away from the film. Application of boundary conditions leads to the implicit dispersion relation $\varepsilon(\omega_Q^+)=-\coth(QD/2)$ for the even parity modes and $\varepsilon(\omega_Q^-)=-\sinh(QD/2)$ for the odd parity modes. As is the case for our rectangular nanowire, for the film the modes for which the electrostatic potential is even under reflection in the x axis lie in the frequency range for which $\varepsilon(\omega)<-1$ and the odd parity modes lie in the range where $-1<\varepsilon(\omega)<0$. The even parity mode of wave vector Q is the twin of the odd parity mode with the same wave vector. The two twins have opposite parity in regard to reflection of the electrostatic potential through the x axis, as in the examples above for the

rectangular nanowire. The even parity mode is often referred to as the acoustic plasmon of the film, since as $Q \to 0$, $\varepsilon(\omega_Q^+) \to \infty$, and ω_Q^+ goes to zero as $Q^{1/2}$. The odd parity mode can be called the optical plasmon mode, since its frequency remains finite at $Q=0$. In this limit, the optical plasmon mode approaches the bulk plasmon frequency of the film, where $\varepsilon(\omega_Q^-) \to 0$.

We next turn to our studies of the response of the rectangular nanowire to an external electric field applied parallel to the long dimension of the cross section. If we consider such a nanowire illuminated by laser radiation, these calculations describe the response of the wire to an appropriately polarized laser beam, in the limit that the linear dimensions of the nanowire are small compared to the wavelength of light.

We begin by presenting studies of Au nanowires of rectangular cross section with aspect ratios chosen to match those studied experimentally in Ref. 11. Thus, we use width to height ratios of 2.56, 4.28, and 7.35, respectively, and in the calculations below it is assumed the nanowires are exposed to an electric field polarized parallel to the long side of the wire. In the calculations presented below, we have used the dielectric constants for Au tabulated by Johnson and Christy.[18]

In Fig. 4(a), we show calculations of the absorption spectra of free standing Au nanowires with the aspect ratios just mentioned. These results have been generated by integrating $\omega\varepsilon_2(\omega)|\vec{E}(\vec{r},\omega)|^2$ over the volume of the wire. We see that as the aspect ratio increases, the absorption peak moves to longer wavelengths. We may compare these spectra with finite difference time (FDTD) calculations of the scattering spectra reported in Fig. 5(c) of Ref. 10. Of course, the peak position in the scattering spectra may not coincide exactly with those in the absorption spectrum, but they should be close. The peak positions in our Fig. 4(a) show trends that compare favorably with those in Ref. 10. For aspect ratios of 3, 5, and 7 these authors find peaks at approximately 520, 580, and 610 nm. We have calculated absorption spectra for these values of the aspect ratio to find peaks at 517, 531, and 570 nm. Both calculations produce very broad spectra, and as the aspect ratio increases we see a substantial shift of the peak to the red. Note that our absorption peaks are shifted to the blue a few percent compared to their calculations of the scattering spectra.

In Fig. 7 of Ref. 9, we see experimental studies of extinction spectra of Au nanowires. Two of the samples have aspect ratios of 2.57 and 4.42, very close to the values used in our Fig. 4(a). The peaks in the extinction spectra are at 540 and 600 nm shifted to the red somewhat from our calculated absorption spectra. It should be remarked that the spectra reported in Ref. 9 are taken from gratings formed from nanowires, but the grating spacing is sufficiently large interwire interaction effects should be modest. One may inquire, as the authors of Ref. 10 discuss, if the redshifts may have their origin in the fact that the nanowires reside on a dielectric substrate. It would be a major challenge to extend our numerical studies to a nanowire which sits on a dielectric substrate. However, we can obtain an upper limit on the substrate-induced shift by fully embedding the nanowires in a dielectric medium. The shifts in the calculated absorption spectra for such a case will be larger than those realized for a sample sitting on a substrate with vacuum above. In Fig. 4(b) we show such calculations and one sees that the redshifts induced by the surrounding dielectric are larger than the discrepancy between the peak positions in Fig. 4(a) and the data of Ref. 9. Thus, it is plausible to attribute the difference between theory and experiment to the influence of the substrate.

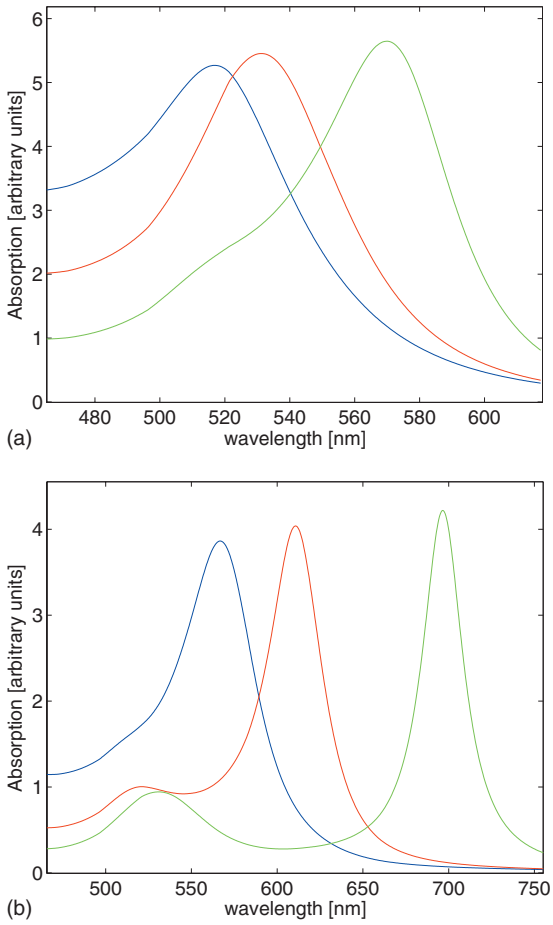

FIG. 4. (Color) We show absorption spectra calculated for Au nanowires of rectangular cross section and with aspect ratios of 2.56 (blue curve), 4.28 (red curve), and 7.35 (green curve). In (a), the nanowire is in vacuum and in (b) it is embedded in a dielectric with dielectric constant of 2.25.

While our calculated absorption spectra have peak positions that compare acceptably with the measured extinction spectra reported in Ref. 9, light scattering studies of similar nanowires reported in both Refs. 10 and 11 show peaks shifted very far to the red compared to the theory presented here and also with the theory presented in Ref. 10. The authors of Ref. 10 suggested that the presence of the substrate might produce such a shift, but we see from our calculations in Fig. 4(b) that the substrate-induced shift is not sufficiently large to explain the discrepancy. The origin of the difference between the two theoretical calculations and the data on these two sets of samples is unclear, unfortunately.

An interesting question is the nature of the enhanced fields that can be realized by exciting the plasmon resonances of the nanowire, along with their spatial distribution around the periphery of the wire. We illustrate this in Fig. 5,

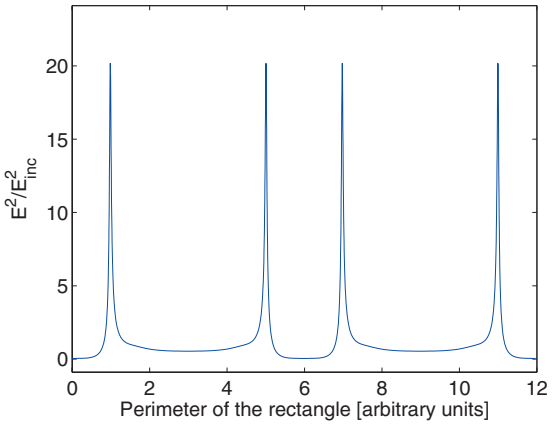

FIG. 5. (Color) The ratio of the square of the electric field just outside a rectangular nanowire to the incident field as a function of position along the outer surface of a rectangular Au nanowire. The aspect ratio is 2:1 and the frequency has been chosen to be at the maximum of the absorption curve. The exciting field is parallel to the long side of the profile of the wire.

where for a nanowire with an aspect ratio of 2, we show the spatial variation of the square of the electric field just outside the wire as a function of position on its surface. The calculations are performed for a frequency at the peak of the absorption curve for this sample. The striking feature of this curve is that the "hot spots" are very clearly very close to the edges of the structure. In our earlier discussion, we saw that right at the corners of the rectangle, we had localized point charges when the plasmons in this frequency regime are excited. The enhanced fields displayed in Fig. 5 are modest in strength largely because Au is a rather lossy material, unfortunately, so the field enhancements one can realize in this material are modest.

There is an interesting message contained in Fig. 5. The hot spots in the nanowire are clearly localized very near the corners. In an actual sample the corners will be rounded to a considerable degree and clearly the field enhancement will be less than expected for the perfectly sharp corners in the ideal profile used to generate Fig. 5. Thus, if one wishes to employ rectangular nanowires in arrays that will be employed to generate enhanced nonlinear optical signals, considerable effort should be devoted to the synthesis of samples with very clean sharp edges. Similar considerations should apply to other nanoscale structures.

The absorption spectra in Fig. 4(a) are dominated by the single lowest frequency mode of the nanowire. This is the mode whose eigenvector is illustrated in Fig. 1(a). On the short wavelength side, in Fig. 4(b) we can see additional structures. It is the case, in fact, that quite a number of modes with frequency higher than the fundamental mode are dipole active and they also have substantial oscillator strengths. We illustrate this in Fig. 6(a). What we have done here is to calculate an absorption spectrum for a Au wire with an aspect ratio of 2. We have artificially reduced the imaginary part of the dielectric constant to a small value. In Fig. 6(b), we plot the absorption spectrum as a function of the real part of the dielectric constant, so for any desired material the frequencies of the various features may be deduced if one had data on the frequency variation of the real part of the dielectric constant.

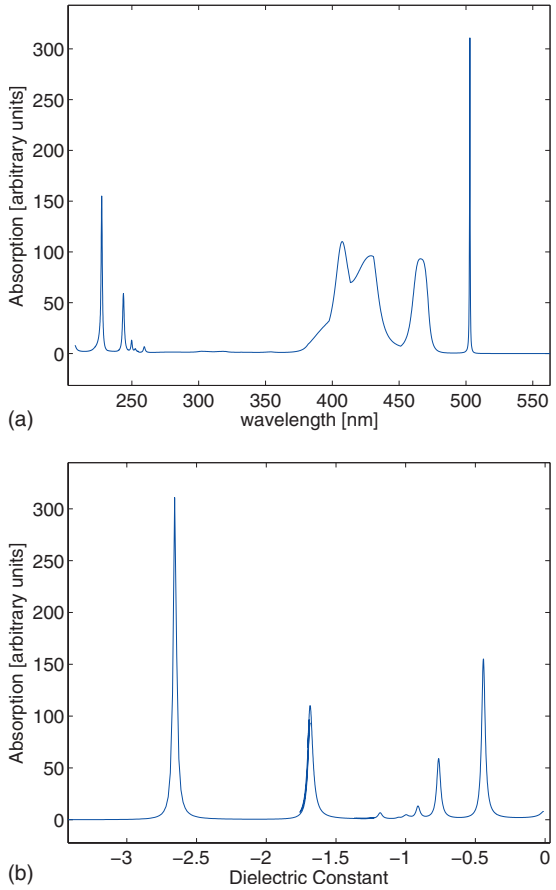

FIG. 6. (Color) (a) The absorption spectrum of a fictitious Au nanowire whose dielectric constant has a small imaginary part. The aspect ratio is 2 and the exciting electric field is parallel to the long side of the cross-sectional area. In this figure the spectrum is plotted as a function of wavelength. See the text for a discussion of the region just above 400 nm. (b) The same as (a), but now the spectrum is plotted as a function of the real part of the dielectric constant.

While the strongest feature in Fig. 6(a) remains the low frequency mode associated with $\varepsilon=-2.655$ (the peak at 515 nm) we see rather intense higher frequency modes. For Au and for the other noble metals, the imaginary part of the dielectric constant is large in this wavelength regime, so these modes do not show as clear features in the absorption spectrum. If one could synthesize conducting nanowires fabricated from low loss conducting materials, it may be possible to realize plasmon enhancement effects at high frequencies.

We wish to comment on the two features in Fig. 6(a) near the wavelength region of 410 nm. We see a doublet here. This doublet in fact has its origin in the same mode, which appears at two different wavelengths in the spectrum. In this spectral regime, the data we have used[17] produce a small broad maximum in the real part of the dielectric constant, so $\varepsilon_1(\omega)$ is not monotonic in this region. Thus, there are two values of the frequency (or wavelength) for which $\varepsilon_1(\omega)$ assumes a value appropriate to one of the dipole active modes.

Since the maximum in the $\varepsilon_1(\omega)$ is a very modest feature, it is not clear to us if this is real or if it is a consequence of very modest errors in the data. It is thus useful to plot the absorption spectrum, calculated with small imaginary part, as a function of ε_1 itself. We show this in Fig. 6(b). The doublet just above 400 nm in Fig. 6(a) has its origin in the mode near $\varepsilon_1=-1.7$ in Fig. 6(b). If one has Au in mind, the spectrum in Fig. 6(b) covers the spectral range from roughly 500 nm up to about 235 nm.

IV. CONCLUDING REMARKS

We have presented a formalism that allows the study of the plasmon normal modes (frequencies and eigenvectors) of nanowires of arbitrary cross-sectional shape. We have used this to examine the nature of the plasmon modes of rectangular nanowires of various aspects along with their response to laser fields. The formalism addresses the electrostatic limit and also assumes the applied external field is spatially uniform. Thus, our attention is directed toward structures whose size is small compared to the wavelength of the radiation which illuminates the wire.

The peaks in our calculated absorption spectra agree with those in the scattering spectra calculated in Ref. 10 by numerical methods. Our results also compare well with the data reported in Ref. 9 save for a relatively small shift to the red compatible to a possible shift whose origin is in the presence of the dielectric substrate. However, while the experimental spectra reported in Refs. 9 and 11 show a shift in the broad peak to the red with increasing aspect ratio similar to what we calculate, our calculated spectra are blueshifted compared to the data.

We show that enhanced fields realized in the idealized Au nanowires we study, where the corners of the cross section are perfectly sharp, are highly localized around these corners. For Au, a rather lossy material, even at the corners the enhanced fields realized are modest. The corners are thus the hot spots and care should be taken to make sharp corners in sample preparation.

It is also the case, as we see from Fig. 6, that the rectangular Au nanowire possesses dipole active plasmon modes that extend to high frequencies beyond the visible. Such modes will be present in diverse nanostructures, clearly. However, the imaginary part of the dielectric constant of the noble metals used widely in experimental studies is large in this spectral region, with the consequence that the modes are very highly damped. It would be of great interest to find a material wherein the absorption is small even in limited frequency regimes in the visible and beyond. One could then design structures whose plasmon modes lie within such frequency bands and realize strong plasmon enhanced response at high frequency. Aluminum is a material where throughout the visible and into the ultraviolet the imaginary part of the dielectric constant is quite small. However, the bulk plasma frequency of aluminum is very high ($\sim$15 eV; its surface plasmon where $\varepsilon=-1$ lies at 10.6 eV) so the plasmon modes of aluminum nano-objects will lie very far out in the ultraviolet. Also oxidation will be a problem, though it should be noted that the presence of an oxide layer shifts the surface plasmon down in frequency to the 7 eV range.[19] It is possible that suitably oxidized aluminum nanostructures could have well defined plasmon resonances in the near ultraviolet. In our view, it would be interesting to see studies of such structures.

ACKNOWLEDGMENTS

We have enjoyed very interesting discussions with E. Potma. The research of D.L.M. was supported by the U.S. National Science Foundation under Grant No. CHE-0802913. A.J. and R.E.A. also acknowledge support from FONDECYT under Contract No. 1085028 (Chile) and from the Millenium Science Nucleus "Basic and Applied Magnetism" under Contract No. P06-022-F (Chile).

[1] For recent review articles, see the volume in K. Kneipp and M. Moskovits, *Surface Enhanced Raman Scattering*, Topics in Applied Physics Vol. 103 (Springer Verlag, Heidelberg, 2006).

[2] J. Steidtner and B. Pettinger, Phys. Rev. Lett. **100**, 236101 (2008).

[3] R. W. Rendell, D. J. Scalapino, and B. Muhlschlegel, Phys. Rev. Lett. **41**, 1746 (1978).

[4] D. L. Mills, Phys. Rev. B **65**, 125419 (2002); Shiwei Wu and D. L. Mills, *ibid.* **65**, 205420 (2002).

[5] P. K. Aravind, A. Nitzan, and H. Metiu, Surf. Sci. **110**, 189 (1981).

[6] P. Chu and D. L. Mills, Phys. Rev. Lett. **99**, 127401 (2007); Phys. Rev. B **77**, 045416 (2008).

[7] R. Arias and D. L. Mills, Phys. Rev. B **68**, 245420 (2003); the theory has been extended to arrays of spheres that exhibit a gyrotropic response to fields in Rodrigo Arias and D. L. Mills, *ibid.* **70**, 104425 (2004); while the topic of this paper is the collective spin-wave modes of arrays of ferromagnetic spheres, the theory can be applied directly to dielectric spheres which exhibit a gyrotropic response.

[8] R. Arias and D. L. Mills, Phys. Rev. B **67**, 094423 (2003); this paper addresses the spin-wave collective modes of ferromagnetic nanowire arrays; however, the theory is directly applicable to the description of plasmons in nanowires. One simply replaces the magnetic permeability tensor by the dielectric tensor, as in discussed in Ref. 10.

[9] G. Schider, J. R. Krenn, W. Gotschy, B. Lamprecht, H. Dillbacher, A. Leitner, and F. R. Aussennegg, J. Appl. Phys. **90**, 3825 (2001).

[10] Q. Xu, J. Bao, F. Capasso, and G. M. Whitesides, Angew. Chem. Int. Ed. **45**, 3631 (2006).

[11] H. Kim, C. Xiang, A. G. Güell, R. M. Penner, and E. O. Potma, J. Phys. Chem. C **112**, 12721 (2008).

[12] D. R. Fredkin and I. D. Mayergoyz, Phys. Rev. Lett. **91**, 253902 (2003).

[13] I. D. Mayergoyz, D. R. Fredkin, and Z. Zhang, Phys. Rev. B **72**, 155412 (2005).
[14] R. Arias and D. L. Mills, Phys. Rev. B **70**, 094414 (2004).
[15] R. Arias and D. L. Mills, Phys. Rev. B **72**, 104418 (2005).
[16] I. D. Mayergoyz, Z. Zhang, and G. Miano, Phys. Rev. Lett. **98**, 147401 (2007).
[17] D. T. DiPerna and T. K. Stanton, J. Acoust. Soc. Am. **96**, 3064 (1994).
[18] P. B. Johnson and R. W. Christy, Phys. Rev. B **6**, 4370 (1972).
[19] D. L. Mills and A. A. Maradudin, Phys. Rev. B **12**, 2943 (1975).